Universiteit Antwerpen

This item is the archived peer-reviewed author-version of:

Correlation between the fluorination degree of perfluorinated zinc phthalocyanines, their singlet oxygen generation ability, and their photoelectrochemical response for phenol sensing

Correlation between the Fluorination Degree of Perfluorinated Zinc Phthalocyanines, their Singlet Oxygen Generation Ability and their Photoelectrochemical Response for Phenol Sensing.

Liselotte Neven[1,2,3], Hanan Barich[1,2], H. Y. Vincent Ching[3], Shahid U. Khan[1,2,4], Christopher Colomier[5], Hemantbhai H. Patel[5], Sergiu M. Gorun[5], Sammy Verbruggen[4], Sabine Van Doorslaer[3], and Karolien De Wael[1,2,*]

[1]A-Sense Lab, Department of Bioscience Engineering, University of Antwerp, Groenenborgerlaan 171, 2020 Antwerp, Belgium; [2]NANOlab Center of Excellence, University of Antwerp, Groenenborgerlaan 171, 2020 Antwerp, Belgium; [3]BIMEF Research Group, Department of Chemistry, University of Antwerp, Universiteitsplein 1, 2610 Wilrijk, Belgium; [4]DuEL Research Group, Department of Bioscience Engineering, University of Antwerp, Groenenborgerlaan 171, 2020 Antwerp, Belgium; [5]Department of Chemistry and Biochemistry and the Centre for Functional Materials, Seton Hall University, 400 South Orange Ave, New Jersey, 07079, USA

ABSTRACT: Electron-withdrawing perfluoroalkyl peripheral groups grafted on phthalocyanine (Pc) macrocycles improve their single-site isolation, solubility and resistance to self-oxidation, all beneficial features for catalytic applications. A high degree of fluorination also enhances the reducibility of Pcs and could alter their singlet oxygen ($^1O_2$) photo-production. The ethanol:toluene 20:80 vol % solvent mixture was found to dissolve perfluorinated F_nPcZn complexes, n = 16, 52 and 64 and minimize the aggregation of the sterically unencumbered $F_{16}PcZn$. The $^1O_2$ production ability of F_nPcZn complexes was examined using 9,10-dimethylanthracene (DMA) and 2,2,6,6-tetramethylpiperidine (TEMP) in combination with UV-Vis and electron paramagnetic resonance (EPR) spectroscopy, respectively. While the photoreduction of $F_{52}PcZn$ and $F_{64}PcZn$ in the presence of redox-active TEMP lowered $^1O_2$ production, DMA was a suitable $^1O_2$ trap for ranking the complexes. The solution reactivity was complemented by solid-state studies via the construction of photoelectrochemical sensors based on TiO$_2$-supported F_nPcZn, $F_nPcZn|TiO_2$. Phenol photo-oxidation by $^1O_2$, followed by its electrochemical reduction define a redox cycle, the $^1O_2$ production having been found to depend on the value of n and structural features of the supported complexes. Consistent with solution studies, $F_{52}PcZn$ was found to be the most efficient $^1O_2$ generator. The insights on reactivity testing and structural-activity relationships obtained may be useful for designing efficient and robust sensors and for other $^1O_2$-related applications of F_nPcZn.

INTRODUCTION

Phthalocyanines (Pcs) are a versatile class of molecules. Their structural variations via changing ring substituents and/or coordinated metals result in different properties and applications. They are used as dyes and pigments, photosensitizers (PS), photodynamic agents, catalysts for photoelectrochemical sensing and photodegradation of contaminants, photovoltaics, etc.[1-5]

Planar Pcs tend to aggregate via π-π stacking, limiting their solubility.[1] However, for optimal photocatalytic efficiency, single-site isolation of the PS is preferred.[6] Indeed, aggregated PSs produce less singlet oxygen ($^1O_2$) due to the shortening of the triplet lifetime and thus inefficient energy transfer to $^3O_2$.[6,7] Tuning the peripheral groups can improve solubility, single-site isolation, photocatalytic reactivity and even increase resistance to self-oxidation. Replacing peripheral, labile C-H bonds by electron-withdrawing substituents, such as F, in zinc 1,2,3,4,8,9,10,11,15,16,17,18,22,23,24,25-hexadecafluoro-29H,31H-phthalocyanine ($F_{16}PcZn$), led to an enhanced resistance against self-oxidation but also to poor solubility in solvents due to stacking.[1,7,8] The generation of single-site isolated species was achieved by introducing bulky i-C_3F_7-groups at the periphery of fluorinated Pc rings, as in zinc(II) 1,4,8,11,15,18,22,25-octafluoro-2,3,9,10,16,17,23,24-octakisperfluoroisopropyl-perfluorophthalocyanine ($F_{64}PcZn$) resulting in an improved solubility in organic solvents, photocatalytic efficiency and chemical and thermal stability.[6,7,9] The introduction of these strongly electron-withdrawing substituents, however, increased the reducibility of the Pc ring,[6] the highly fluorinated Pcs being more susceptible to electrochemical reduction relative to $H_{16}PcZn$.[9] In view of this characteristic, it is worth to investigate how this reducibility feature can influence the $^1O_2$ production of the PS.

Strategies to detect $^1O_2$ in solution are based on direct or indirect methods. The most direct detection of $^1O_2$ involves its 1270 nm phosphorescence signal measured with time-resolved near-infrared (TRNIR) emission spectroscopy and gives unambiguous results on the $^1O_2$ production of the PS. Yet, its application is not trivial; this complex method requires expensive equipment, being in contrast with the more feasible indirect methods.[10, 11] Hence, in this report we focussed on assessing indirect methods involving the trapping of $^1O_2$ by chemicals (i.e. probes). In these methods, a probe reacts with $^1O_2$ and the degradation of the probe or formation of a product is monitored via a specific detection method.[12] Examples of these probes include sterically hindered cyclic amines such as 2,2,6,6-tetramethylpiperidine (TEMP) combined with electron paramagnetic resonance (EPR) spectroscopy[11, 13, 14] or 9,10-dimethylanthracene (DMA) with UV-Vis detection[15-18] (Figure S1). Importantly, these experiments rely on the fact that the degradation of the probe or the formation of a detectable compound is solely dependent on the $^1O_2$ production and are not influenced by other mechanisms. Other reaction paths cannot always be excluded. As stated by Nardi *et al.*,[11] a PS may oxidize TEMP via electron transfer, if the process is thermodynamically allowed, which can also lead to the generation of 2,2,6,6-tetramethylpiperidine 1-oxyl (TEMPO) even though there is no involvement of $^1O_2$. In fact, they even showed that the addition of tris(4-bromophenyl)aminium hexachloroantimonate (BAHA), an oxidizing agent, also leads to the generation of TEMPO.

In light of this, it is crucial to evaluate how the reducibility of highly fluorinated ZnPcs influences the $^1O_2$ determination by indirect methods, if electron transfer reaction occurs with easily oxidizable probes such as TEMP, and how the high fluorination degree influences their $^1O_2$ production in solution and in solid state (deposited on a matrix).

Therefore, in this article, the $^1O_2$ production by ZnPc complexes $H_{16}PcZn$, $F_{16}PcZn$, $F_{52}PcZn$ and $F_{64}PcZn$ exhibiting an increased fluorination degree (Figure 1) are compared. DMA in combination with UV-Vis measurements and the easily oxidizable probe TEMP with EPR spectroscopy are used to probe $^1O_2$ production. The obtained data are correlated with the sensitivity obtained in a photoelectrochemical sensor since the specific micro-environment can also influence the $^1O_2$ production, due to the deposition of the PS on a TiO_2 matrix or the reaction with analytes. Comparing the $^1O_2$ production of different ZnPc derivatives is important for its application as the choice of the highest $^1O_2$ generator is beneficial for the sensitivity of the photoelectrochemical sensor.

EXPERIMENTAL

Materials. $H_{16}PcZn$ and $F_{16}PcZn$ were purchased from TCI and Sigma Aldrich, respectively. $F_{52}PcZn$, $F_{64}PcZn$ and $F_{52}PcZn$ and triphenyl phosphine oxide, $OPPh_3$ in toluene (used to gain atomic-level structural information) were synthesized as described in Supporting Information. The PSs were immobilized on a TiO_2 P25 support with loadings of 3 wt %. The supported PSs are abbreviated as $H_{16}PcZn|TiO_2$, $F_{16}PcZn|TiO_2$, $F_{52}PcZn|TiO_2$ and $F_{64}PcZn|TiO_2$. Ethanol (EtOH), and toluene were purchased from Fisher Chemical and Acros Organics, respectively. The used solvent system was 20:80 vol % EtOH:toluene. TEMP and DMA were obtained from Sigma Aldrich and TCI, respectively. Phenol and catechol were purchased from J&K Scientific. Sodium
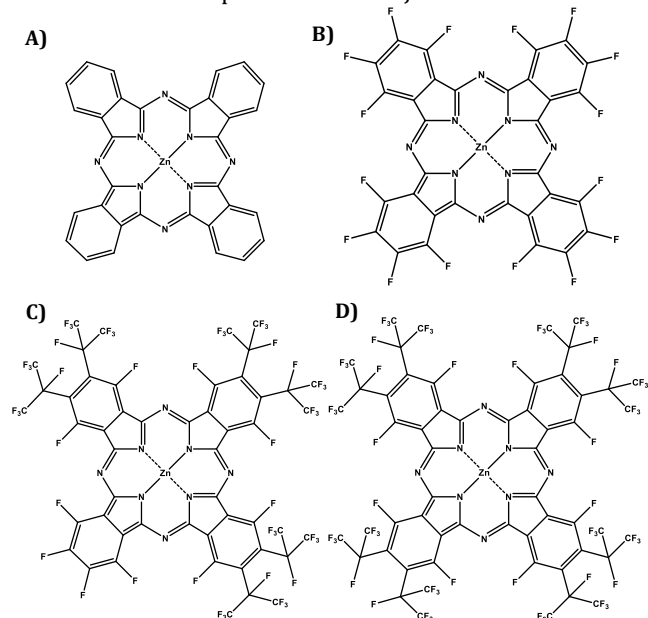

Figure 1. Molecular structures of $H_{16}PcZn$ (A), $F_{16}PcZn$ (B), $F_{52}PcZn$ (C) and $F_{64}PcZn$ (D).

phosphate and potassium chloride were obtained from Sigma-Aldrich and Acros Organics. Boric acid was purchased from Merck. A diode laser, from Roithner Lasertechnik, operating at 655 nm was used as an illumination source. The laser power was measured at the sample position and was set to 0.16 W cm^{-2} for the EPR and UV-Vis measurements and 0.24 W cm^{-2} for the $^1O_2$-based sensing of phenolic compounds. No lenses were used.

UV-Vis measurements. UV-Vis measurements were performed on an Avantes AvaSpec-2048L spectrophotometer. The extinction coefficients of the PSs (Table S1) were calculated by the slope of the absorbance as a function of the PS concentration. The PS absorbance of 0.12 at 655 nm in 20:80 vol % EtOH:toluene was chosen to minimize the contribution of the Pc's B band to the DMA bands (Figure S2) that was used for quantifying $^1O_2$ production. This increases the precision of $^1O_2$ determination using DMA. The absorbance values were consistent with the following concentration of the PSs: 3.4 μmol L^{-1} ($H_{16}PcZn$), 2.4 μmol L^{-1} ($F_{16}PcZn$), 3.2 μmol L^{-1} ($F_{52}PcZn$) and 4.0 μmol L^{-1} ($F_{64}PcZn$). Cuvettes of 2 mL (1 cm x 1 cm) and 250 μL (1 mm x 1 cm) were used (cap size was 1 cm x 1 cm). The cuvettes were closed to avoid evaporation of the solvent during the experiments. The UV-Vis spectra of the probes DMA and TEMP were also recorded as a control reference (Table S1 and Figure S3). For $^1O_2$ detection, 125 μmol L^{-1} DMA was added to the solution containing the PS in 20:80 vol % EtOH:toluene. A 2 mL quartz cuvette (1 cm x 1 cm) was used and the 655 nm laser beam (0.16 W cm^{-2}) was positioned perpendicular to the optical path. The solution was magnetically stirred. A first UV-Vis spectrum was taken without illumination, followed by spectra taken every minute for a total illumination time of 10 minutes. The decrease of the intensity of the 380 nm band of DMA was used to follow its peroxidation. Catechol, 50 mmol L^{-1}, was added to the solution containing the PS and DMA to quench the produced $^1O_2$.

EPR measurements. Room temperature X band continuous-wave EPR experiments were conducted on a Bruker ESP300E spectrometer equipped with a TE_{103} mode ER4104OR optical transmission resonator, operating at X-band (~9.4 GHz) microwave frequency. Spectra were collected at room temperature using 20 mW microwave power with a modulation amplitude and frequency of 0.1 mT and 100 kHz. The scan time was 40 seconds over a range of 8 mT. The 655 nm laser (0.16 W cm^{-2}) was positioned 30 cm from the EPR cavity. Solutions of 200 μL 20:80 vol % EtOH:toluene of 100 mmol L^{-1} TEMP and the PS (optical absorbance of 0.12 at 655 nm) were prepared. Each sample was mixed subsequently an aliquot of 25 μL was transferred into a capillary (1 mm inner diameter) which was then placed inside a 4 mm EPR tube and loaded into the EPR cavity. The first EPR spectrum was taken without illuminating the solution and a second spectrum was taken after three minutes illumination to evaluate the increase in the EPR signal of TEMPO. The signal area was determined by taking the double integral of the spectrum which correlates with the number of spins. By comparison with a calibration plot based on the EPR spectra of different concentrations of TEMPO in 20:80 vol % EtOH:toluene, the amount of produced TEMPO could be determined in each PS solution. To test whether $^1O_2$ was the cause of TEMPO formation, 50 mmol L^{-1} catechol was added to the solution containing the PS and TEMP to quench the produced $^1O_2$.

UV-DR measurements. UV-diffuse reflectance (UV-DR) experiments were conducted on the Shimadzu UV2600 UV-Vis spectrophotometer. Approximately 3 to 5 mg of PS|TiO$_2$ powder was spread over a pellet of BaSO$_4$. The obtained spectra were compared with the spectrum of TiO$_2$ P25.

Photoelectrochemical sensor. *Modification of the electrode surface with PS/TiO$_2$.* ItalSens and Metrohm DropSens graphite screen-printed electrodes (SPEs) were purchased from PalmSens and Metrohm. The SPEs consisted of a silver pseudo-reference, carbon counter electrode and graphite working electrode (WE) of 3 mm diameter for ItalSens and 4 mm for Metrohm. The WE was coated with 3 wt % PS|TiO$_2$ by casting: a small droplet of an aqueous 10 mg mL^{-1} PS|TiO$_2$-suspension was placed on the WE surface and left to dry overnight resulting in a PS|TiO$_2$-coated SPE. To deposit 1.5 μg PS (0.05 mg PS|TiO$_2$) on the WE surface, 5 μL of an aqueous PS|TiO$_2$-suspension was deposited. To drop-cast 0.73 nmol PS, 1.40, 2.10, 4.27 and 5.00 μL from an aqueous suspension of H$_{16}$PcZn|TiO$_2$, F$_{16}$PcZn|TiO$_2$, F$_{52}$PcZn|TiO$_2$ and F$_{64}$PcZn|TiO$_2$, respectively, was needed. At last, 3.75 and 5 μL were drop-casted on the working electrode surface from an aqueous suspension of, respectively, F$_{52}$PcZn|TiO$_2$ and F$_{64}$PcZn|TiO$_2$ to obtain coatings with an optical absorbance of 0.015 at 655 nm. The amount of drop-casted PS was calculated based on the UV-DR spectra of F$_{52}$PcZn|TiO$_2$ and F$_{64}$PcZn|TiO$_2$ in relation to the UV-Vis spectrum of these PS's in 20:80 vol % EtOH:toluene.

Photoelectrochemical measurements. The photoelectrochemical measurements were conducted using a μAutolab III (Metrohm Autolab) instrument with NOVA software. The buffer solution was a phosphate buffer consisting of 0.02 mol L^{-1} KH$_2$PO$_4$ and 0.1 mol L^{-1} KCl dissolved in ultrapure water. The pH was adjusted with KOH. The measurements were performed in an 80 μL droplet consisting of either phosphate buffer (blank) or 10 μmol L^{-1} phenol in phosphate buffer. A potential of -0.10 V vs Ag pseudo-reference electrode was applied during amperometric measurements. The Ag pseudo-reference electrode of the SPE had a potential of approximately +0.05 V versus SCE. The values of the potentials are given versus the Ag pseudo-reference electrode of the SPE, if not mentioned otherwise. The limit of detection (LOD) of phenol was calculated by the ratio of 3 times the standard deviation of the blank to the gradient of the calibration curve. This calibration curve was established at -0.14 V vs Ag pseudo-reference and pH 9 borate buffer (0.02 mol L^{-1} H$_3$BO$_3$ and 0.1 mol L^{-1} KCl). The 655 nm laser (0.24 W cm^{-2}) was switched on and off at specific time intervals. The first illumination was used to adjust the laser's beam position to fully cover the WE surface.

RESULTS AND DISCUSSION

Structural features of the PSs. The structures of the PSs are shown in Figure 1. Single-site isolation of the PS is crucial to achieve high $^1O_2$ production yields and optimal photocatalytic activities both in solution and in the solid-state.[1, 6, 7] Aggregation, due to π-π stacking decreases the triplet lifetime of excited PS and thus lowers their $^1O_2$ production.[7] Planar structures, devoid of bulky substituents favour stacking while, from an electronic point of view, a decrease of the π electronic density of macrocyclic rings has the same effect. Thus, H$_{16}$PcZn is less aggregated than F$_{16}$PcZn, both molecules being planar.[19] The i-C$_3$F$_7$ groups of F$_{64}$PcZn have been shown to prevent aggregation due to steric hindrance, both in solution and in the solid-state.[20] There is, however, an additional factor that may prevent aggregation via π-π stacking: axial coordination. F$_n$PcZn coordinate oxygen-based ligands, including acetone, methanol, ethanol and water via Zn-O bonds.[6] In addition to preventing stacking, axial ligation, resulting in 5-coordination, distorts the Pc ring slightly, while 6-coordination, i.e. 2 axially bonded ligands does not. Notable, F$_{16}$PcZn is almost planar in the solid state in the absence of axial ligands.[21] F$_{52}$PcZn is a special case, having 1 quadrant like F$_{16}$PcZn-like and 3 quadrants F$_{64}$PcZn-like, Figure 1. The Zn-coordination by O-ligands is of interest and is illustrated by the single-crystal X-ray structure of F$_{52}$PcZn-O-R*3Toluene, where R is PPh$_3$. Structural details are shown in Figure S4.

The F$_{52}$PcZnOPPH$_3$*3Toluene contains both an oxygen ligand and toluene, a solvent used for the reported studies. However, as anticipated, toluene is not directly bonded to the Pc complex, although it does exhibit π stacking interactions. Both oxygen axial ligands and toluene may be thus useful to solubilize the complexes, as revealed by solution studies.

These results suggest that the F$_n$PcZn may be directly ligated to a hydroxyl group of TiO$_2$. The proximity of the Pc to the electrode surface, as well as the availability of the 6th Zn-coordination site, open for possible substrate coordination, might facilitate both the oxidation and reduction of analytes. While F$_{16}$PcZn will lead to the least steric hindrance for oxygen-mediated ligation to TiO$_2$, the high alkyl fluorine content in F$_{64}$PcZn will favour the binding of the electron lone pair to oxygen to the electron-poor metal site most, but

hamper it sterically. $F_{52}PcZn$ may in this respect offer an optimum between $F_{16}PcZn$ and $F_{64}PcZn$. As seen in Figure S4, the P bonded to the Zn-coordinated oxygen is located above the F atoms of the i-C_3F_7 groups. This geometry, along with the slight doming of the Pc macrocycle due to the 5-coordination does not rule out the axial coordination to the Zn of a surface oxygen of an inorganic oxide.

It is important to note that axial coordination has a minimum effect on the HOMO-LUMO gap and thus the position of the Q-bands. The above structural considerations are relevant to solution and electrode-based studies, discussed next.

Spectroscopic properties and stability of the PSs in solution. The extinction coefficients of the PSs are reported in Table S1. Choosing the appropriate solvent is essential to obtain isolated PS species. Though, $H_{16}PcZn$ is soluble in dimethyl sulfoxide and toluene,[22, 23] $F_{16}PcZn$ has a low solubility in most polar and non-polar solvents and, when solubilized, its aggregated form is mainly present.[1, 24] A mixed solvent system, 20:80 vol % EtOH:toluene, was found to be suitable for spectroscopic studies in solution since toluene ensures the solubility of the PS[6] while the presence of EtOH prevents aggregation by coordination to the Zn ion,[8, 25] in agreement with the above structural discussion.
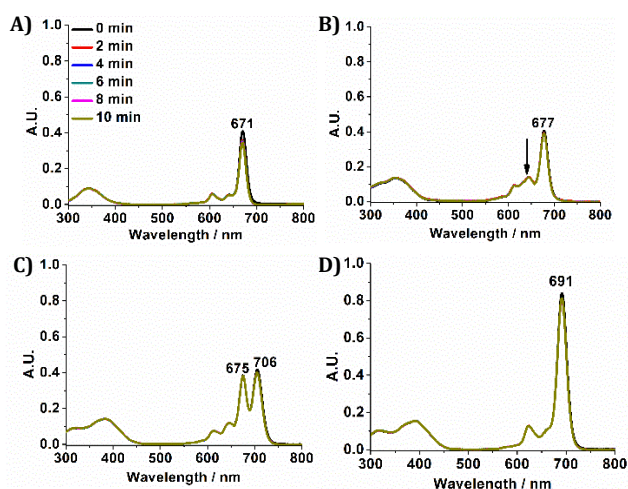

Figure 2. Absorbance spectra of $H_{16}PcZn$ (A), $F_{16}PcZn$ (B), $F_{52}PcZn$ (C) and $F_{64}PcZn$ (D) in 20:80 vol % EtOH:toluene during 10 minutes illumination with 655 nm laser in aerobic condition. Absorbance of the PS was 0.12 at 655 nm. A cuvette of 2 mL was used (1 cm x 1 cm, capped). Overlays of spectra recorded at 0, 2, 4, 6, 8 and 10 minutes illumination of F_nPcZn are shown.

The optical spectra of F_nPcZn in the mixed ethanol:toluene solvent, Figure 2, exhibit narrow Q bands and the absence of blue-shifted bands, suggesting the predominance of single-sites for $H_{16}PcZn$, $F_{52}PcZn$ and $F_{64}PcZn$. As expected, the Q band shifts from 671 nm ($H_{16}PcZn$) to 691 nm ($F_{64}PcZn$) as the fluorination degree of the structure increases. In the case of $F_{52}PcZn$, the Q band is split due to the loss of 4-fold symmetry of the complex.[2, 26] The UV-Vis spectrum of $F_{16}PcZn$ proved that a small amount of the PS was aggregated by the presence of a blue-shifted band at 645 nm (indicated by the arrow in Figure 2.B). So, the solubility of the ZnPc derivatives in this solvent was the least for $F_{16}PcZn$.

During a 10 minutes illumination period, $H_{16}PcZn$ had the highest decrease in Q band intensity, i.e. 16 %, indicating some bleaching of the PS. In contrast, the peripheral electron-withdrawing groups increase the resistance against self-oxidation by $^1O_2$[8, 9] for $F_{16}PcZn$, $F_{52}PcZn$ and $F_{64}PcZn$. A decrease of the Q band absorbance of only 3 to 4 % was noted during that illumination period and, thus, confirmed the chemical inertness of these ZnPc derivatives to the $^1O_2$ they produce.

Detecting $^1O_2$ using UV-Vis with DMA probe. The $^1O_2$ production efficiency of the PSs was evaluated by UV-Vis measurements with the probe DMA. DMA produces a distinctive UV-Vis spectrum with three bands in the 300 – 420 nm region (Figure S3.A and S2). Its oxidation by $^1O_2$ leads to the decrease of these UV-Vis bands as a function of the illumination time, due to the formation of an *endo*-peroxide (Figure S1), and follows a first order kinetic.[16, 18]

The peroxidation of DMA was followed during a 10 minutes illumination period with a 655 nm laser and a significant decrease in the DMA absorbance bands was observed (Figure S5 and S6). $H_{16}PcZn$ had the fastest rate in oxidizing DMA which resulted in 89.2 % consumption of the initial DMA concentration after 10 minutes (Table 1, Figure S6.A). A similar rate constant was determined for $F_{52}PcZn$ which resulted in 84 % of the DMA concentration being peroxidised. $F_{64}PcZn$ had a 1.2 times smaller rate constant than $F_{52}PcZn$ but could still peroxidise up to 80 % of DMA. The lowest peroxidation rate constant was obtained with $F_{16}PcZn$ where only 73 % of the initial DMA concentration was consumed after 10 minutes illumination. This lowered photoactivity is likely the result of aggregation of the PS in the solvent (Figure 2.B), lowering its triplet lifetime.[7] Indeed, in acetone and the absence of oxygen, a similar observation was made, the triplet lifetime of $F_{64}PcZn$ was 52 μs while for $F_{16}PcZn$ this was < 1 μs due to aggregation.[8]

The specificity of the DMA oxidation by $^1O_2$ was confirmed by evaluating the UV-Vis spectra of the PSs (Figure S5). No indication of a reaction between DMA and the PS was observed since the UV-Vis bands of the PSs were similar as in the absence of DMA and were not altered during the illumination period. The addition of catechol in the UV-Vis measurements (Figure S6.B) decreased the peroxidation kinetic 1.9, 1.6, 2.4 and 2.5 times for $H_{16}PcZn$, $F_{16}PcZn$, $F_{52}PcZn$ and $F_{64}PcZn$ respectively, after 5 minutes illumination. So, the peroxidation of DMA is caused by the $^1O_2$ generation of the PS in 20:80 vol% EtOH:toluene and the differences in the peroxidation rate and DMA consumption are the result of their particular $^1O_2$ production activities.

Table 1. DMA peroxidation parameters for the ZnPc derivatives (N = 3) during 10 minutes illumination with 655 nm laser in air. Added concentration of DMA was 125 μmol L^{-1}. Optical absorbance of the PS at 655 nm was 0.12 in 20:80 vol% EtOH:toluene.

Photocatalyst	Rate constant for DMA peroxidation, min^{-1}	DMA consumption[a] (after 10 min), %
$H_{16}PcZn$	0.238 ± 0.004	89.2 ± 0.1
$F_{16}PcZn$	0.138 ± 0.002	73.0 ± 0.6
$F_{52}PcZn$	0.228 ± 0.006	84 ± 1
$F_{64}PcZn$	0.190 ± 0.001	80.3 ± 0.4

These results are consistent with previous $^1O_2$ production in ethanol, using (S)-(–)-Citronellol, abbreviated ((S)-Cit.) as a trap, Table S2.

$^1O_2$ detection via spin-trap EPR. *TEMPO formation by F_nPcZn.*

The evaluation of the $^1O_2$ production efficiency of the PSs obtained via the peroxidation with DMA were compared with the results obtained using an EPR method. The oxidation of TEMP by $^1O_2$ leads to the EPR-active TEMPO (Figure S1) which gives a characteristic three-line EPR signal with 1:1:1 intensities arising from the ^{14}N (*I*=1) hyperfine coupling.[11] Prior to the addition of the PS, a small EPR signal of TEMPO that does not increase upon illumination, is detected for TEMP in 20:80 vol % EtOH:toluene (Figure S7).
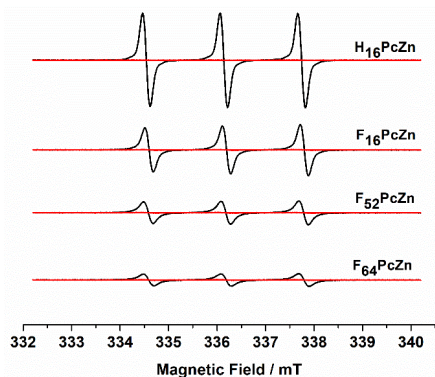

Figure 3. X-band EPR spectra of TEMPO formed by $H_{16}PcZn$ and F_nPcZn, n = 16, 52 and 64, in 20:80 vol % EtOH:toluene from TEMP (100 mmol L^{-1}) at 0 (red) and 3 (black) minutes illumination with 655 nm laser. The amount of PS corresponded to an absorbance of 0.12 at 655 nm. The spectra are depicted scaled such as to reflect their relative difference in peak intensity.

A significant increase in the TEMPO signal was observed in the presence of the PS after three minutes illumination (Figure 3). The light-induced TEMPO EPR signal depends on the fluorination degree. $H_{16}PcZn$ produced the highest amount of TEMPO, e.g. 0.45 mmol L^{-1} TEMPO, followed by $F_{16}PcZn$ 0.31 mmol L^{-1} TEMPO. The lowest amount of TEMPO was obtained in the presence of $F_{52}PcZn$ and $F_{64}PcZn$; respectively, 0.24 mmol L^{-1} and 0.13 mmol L^{-1} TEMPO was produced. So, as in the peroxidation of DMA, $H_{16}PcZn$ produces the most $^1O_2$. Nevertheless, a different trend for the $^1O_2$ production of $F_{16}PcZn$, $F_{52}PcZn$ and $F_{64}PcZn$ was obtained with EPR compared to UV-Vis. A plausible explanation for this observed difference in photoactivity is the degradation of the PS itself by reaction with TEMP since, as shown before, the PSs itself are stable in function of the illumination time and in the presence of DMA (Figure 2 and S5).

Photoinduced electron transfer between TEMP and F_nPcZn.

The aromatic C-H and C-F bonds to aliphatic perhalogenated substituents increase the chemical susceptibility of the Pc towards oxidizable species.[6, 9] TEMP, a possible reducing agent (E_{ox} = 1.0 V vs SCE[11]), could, therefore, reduce highly fluorinated Pcs. More specifically, the photoreduction of $F_{64}PcZn$ by nitrogen-containing molecules, such as hydrazine hydrate, has already been observed.[6] The possibility of a reaction between TEMP and the PS was evaluated by UV-Vis measurements (Figure 4).
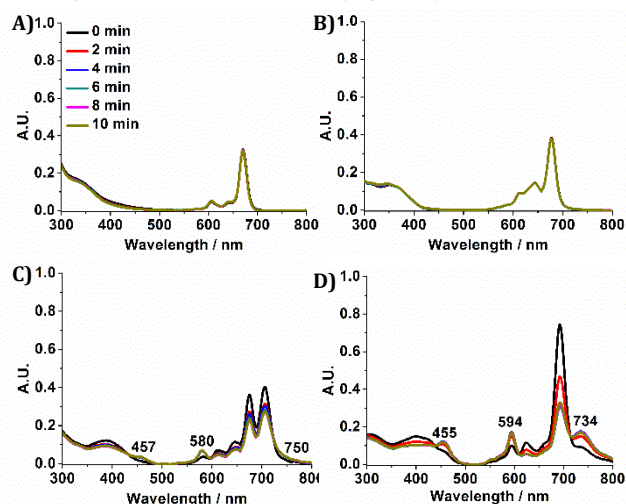

Figure 4. Overlay of UV-Vis spectra, recorded at 0, 2, 4, 6, 8 and 10 minutes illumination, of $H_{16}PcZn$ (A), $F_{16}PcZn$ (B), $F_{52}PcZn$ (C) and $F_{64}PcZn$ (D) in the presence of 100 mmol L^{-1} TEMP in 20:80 vol % EtOH:toluene in aerobic condition. Total illumination period with a 655 nm laser was 10 minutes. Absorbance of PS at 655 nm was 0.12. A cuvette of 2 mL was used (1 cm x 1 cm, capped).

The addition of TEMP did not alter the absorbance bands of $H_{16}PcZn$ and $F_{16}PcZn$ in function of the illumination time (Figure 4.A and B). There was no indication of a reaction between TEMP and these Pcs. Therefore, it is expected that their $^1O_2$ production in the peroxidation of DMA and oxidation of TEMP can be directly compared.

However, the absorbance bands of $F_{52}PcZn$ and $F_{64}PcZn$ changed noticeably in the presence of TEMP (Figure 4.C and D). New bands around 580 nm and a shoulder at 750 nm for $F_{52}PcZn$ and, 594 nm and 734 nm for $F_{64}PcZn$ appeared and increased during the illumination period. The B band also shifted towards 457 nm for $F_{52}PcZn$ and 455 nm for $F_{64}PcZn$. The intensity of the Q bands decreased over the illumination period 34 % for $F_{52}PcZn$ while for $F_{64}PcZn$, a lowering in intensity of 61 % was noted. Interestingly, this diminishing feature of $F_{64}PcZn$ was already obtained after three minutes illumination. It suggests that when the EPR measurement was performed, the absorbance of the Q band was approximately 26 % and 61 % lowered for $F_{52}PcZn$ and $F_{64}PcZn$, respectively, with a decreasing absorbance of 23 % and 33 % at the laser wavelength as a result.

The altered UV-Vis spectrum of $F_{52}PcZn$ and $F_{64}PcZn$ resembles the UV-Vis spectrum of the photoreduced Pc.[6] The presence of fluoroalkyl electron-withdrawing groups in $F_{52}PcZn$ and $F_{64}PcZn$, facilitate the (photo)reduction of the Pc complex and is likely the result of an electron transfer from TEMP to the excited PS (photoinduced electron transfer, PET) leading to the generation of the radical cation TEMP$^{•+}$ and the photoreduced Pc complex [Pc]$^{•-}$.[6, 11] Moreover, as the fluorination degree increased from $F_{52}PcZn$ to $F_{64}PcZn$, this photoreduction by TEMP became more pronounced. This photoreduction partially occurred when there was no laser illumination (black line, Figure 4.C and D), indicating that scattered daylight was already sufficient to photoreduce $F_{52}PcZn$ and $F_{64}PcZn$ by TEMP.

UV-Vis measurements of the Pcs in the presence of TEMPO showed no photoreduction of the Pc and, therefore, exclude that the photoreduction was by TEMPO binding instead of TEMP binding and subsequent further oxidation of TEMPO (Figure S8).

It should be emphasized, however, that the EPR measurement conditions are significantly different from the UV-Vis measurement conditions. More specifically, since the EPR measurements occurred inside a capillary, the only available O_2 for $^1O_2$ production was in the vicinity of the PS while for the UV-Vis measurements diffusion of O_2 took place. Therefore, depletion of O_2 might occur in the EPR tubes as more $^1O_2$ was produced, possibly increasing the photoreduction of $F_{64}PcZn$ and $F_{52}PcZn$. Such an effect was observed for $F_{64}PcZn$ in EtOH during red light illumination in the absence of air (N_2 atmosphere) by Moons et al.[6]

When the UV-Vis measurements of the PSs were taken in a cuvette of 250 μL volume where the only available O_2 for $^1O_2$ production was mainly in the vicinity of the PS, no photoreduction of the PS was observed (Figure S9). Only upon the addition of TEMP, photoreduction of $F_{52}PcZn$ and $F_{64}PcZn$ occurred (Figure S10). This is in agreement with Moons et al., where the photoreduction of the PS in N_2 atmosphere was not observed in non-coordinating solvents such as toluene.[6]

The generation of the radical cation TEMP$^{•+}$ could lead to the formation of TEMPO, if the electron transfer reaction is followed by a deprotonation of the amine group of TEMP and reaction with molecular oxygen.[11] Thus, beside the TEMPO generated via $^1O_2$, a second pathway can also contribute to the TEMPO EPR intensity. In that case, it is expected that the TEMPO EPR signal should increase with increasing fluorination degree, as the susceptibility for reduction increases, which was not observed in Figure 3. Moreover, the TEMPO signal was extensively lower at three minutes illumination when a $^1O_2$ quencher, catechol, was added to the solution (Figure 5), proving the involvement of $^1O_2$ in the TEMPO formation. If the TEMPO EPR signal originated from a PET reaction, then the signal should remain unaltered in the presence of the quencher.[11, 13] The results in Figure 5 exclude that electron transfer between TEMP and $F_{52}PcZn$ and $F_{64}PcZn$ leads to the formation of TEMPO.
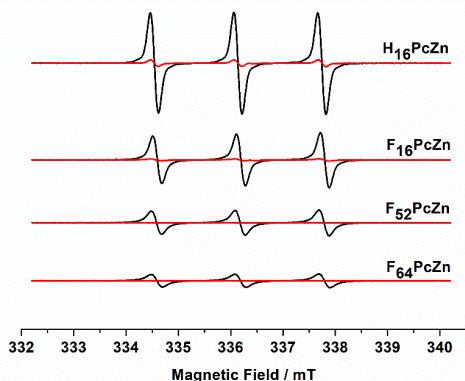

Figure 5. X-band EPR spectra of TEMPO formed by $H_{16}PcZn$ and F_nPcZn, n is 16, 52, 64, in 20:80 vol % EtOH:toluene from TEMP (100 mmol L^{-1}) in the presence (red) and absence (black) of 50 mmol L^{-1} catechol after 3 minutes illumination with 655 nm laser. The amount of PS corresponded to an absorbance of 0.12 at 655 nm.

Though not observed in this case, the generation of TEMPO via PET reactions has been described in literature[11] in aerated solutions. This aeration probably enhanced the reaction of molecular oxygen with TEMP$^{•+}$ leading to the generation of TEMPO.

In conclusion, when comparing the different $^1O_2$ detection techniques, the trends established by the trap DMA provide the correct representation of the $^1O_2$ production capabilities of F_nPcZn, while the use of TEMP for EPR measurements leads to the photoreduction of $F_{52}PcZn$ and $F_{64}PcZn$ with a lowered $^1O_2$ production as a result. Similarly sterically hindered secondary amines[13, 14, 27, 28] could easily reduce highly fluorinated PSs under illumination and thus render the EPR probe unreliable. Nonetheless, based on the DMA experiments, the ranking of the Pc compounds as good PS is $H_{16}PcZn$ and $F_{52}PcZn$, followed by $F_{64}PcZn$ and $F_{16}PcZn$. Notably, however, is the degradation of $H_{16}PcZn$ under illumination, the only non-fluorinated PS.

$^1O_2$-based sensing: photoelectrochemical detection of phenol. The Pc derivatives were deposited on a TiO_2 carrier matrix, containing nm-size particles, for their use in $^1O_2$-based photoelectrochemical sensing of the model compound phenol (Figure S11).[4, 5] In this sensor, the PS|TiO_2-coated WE is illuminated by a red laser leading to the production of $^1O_2$. This latter compound oxidizes phenol, present in the droplet on the electrode, leading to the generation of benzoquinone (BQ). The subsequent reduction of BQ at the electrode surface leads to the formation of hydroquinone (HQ) which can be oxidized again by $^1O_2$ and completes the redox cycle.[4, 5] This photoelectrochemical sensor measures the total phenol amount in a sample, similar as existing techniques for phenol detection, i.e. COD measurements and 4-aminoantipyrine color tests.[29, 30]

As concluded in the previous paragraph, it is expected that the PS|TiO_2-coatings containing the PSs $H_{16}PcZn$ and $F_{52}PcZn$ should give the highest sensitivity in the sensor since they have the highest photoactivity in solution. It should lead to an increased amount of oxidized phenolic compounds and, as a result, an elevated response. However, if the PSs are aggregated on the TiO_2 surface, a diminishing $^1O_2$ production can be expected due to the shortening of the triplet lifetimes.[7] Thus, before the coatings are subjected to the photoelectrochemical detection of phenol, the potential aggregation of the PSs on TiO_2 was first analysed by UV-DR measurements (Figure 6).
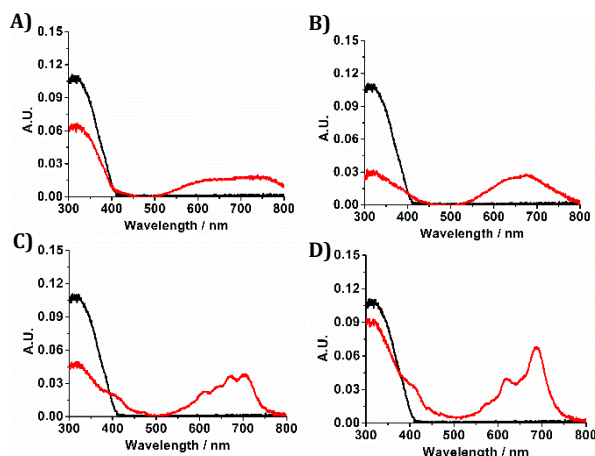
Figure 6. UV-DR spectrum of 3-5 mg of TiO₂ P25 (black) and 3 wt % $H_{16}PcZn|TiO_2$ (A), $F_{16}PcZn|TiO_2$ (B), $F_{52}PcZn|TiO_2$ (C) and $F_{64}PcZn|TiO_2$ (D) presented in red.

All spectra showed the intrinsic absorbance band of TiO₂ below 400 nm. The UV-DR spectrum of $F_{52}PcZn|TiO_2$ (Figure 6.C) and $F_{64}PcZn|TiO_2$ (Figure 6.D) showed the characteristic but relatively broad Q bands in the same 600-750 nm region as the PS in solution. The B bands were also observed in the 400 nm region overlaying the signal from TiO₂. Therefore, it seems that $F_{52}PcZn$ and $F_{64}PcZn$ are well dispersed over the TiO₂ particles resulting in single-site isolation which is necessary for high photocatalytic activity.

However, for $H_{16}PcZn|TiO_2$ and $F_{16}PcZn|TiO_2$, the characteristic Q bands and B band were not observed (Figure 6.A and B). Only a broad band ranging from 550 to 800 nm was observed. The absence of the Pc's characteristic optical bands could be the result of destruction of the PS, which would occur during the deposition on TiO₂ and the drying in the oven or (more likely) the result of aggregation of the PS on the TiO₂ surface. To understand why the characteristic Q band was absent, leaching experiments were performed on $H_{16}PcZn|TiO_2$ and $F_{16}PcZn|TiO_2$ with 20:80 vol % EtOH:toluene. Approximately 90 % and 55 % for respectively $H_{16}PcZn|TiO_2$ and $F_{16}PcZn|TiO_2$ was leached (Figure S12). UV-Vis spectra, taken from the leached PS solution, showed the characteristic absorbance bands of these PSs. The features in the UV-Vis spectra were identical as when the PS was solubilized in the same solvent. Therefore, it seems that there was no degradation of the PS and that the UV-DR spectra corresponded to aggregated clusters of $H_{16}PcZn$ and $F_{16}PcZn$ on the TiO₂ surface probably formed during the solvent evaporation step of the deposition. The lower amount of leaching of $F_{16}PcZn$ was probably caused by its lower solubility in 20:80 EtOH:toluene. Although the broadened bands in the UV-DR spectra of $F_{52}PcZn|TiO_2$ and $F_{64}PcZn|TiO_2$ may also point to some aggregation, the effect is considerably lower than for the other two systems.

Next, the different PS|TiO₂-coatings were used for the photoelectrochemical detection of phenol (Figure S11). The photocurrent responses of the different PS|TiO₂-coatings (Figure S13) were compared when equal PS moles, 0.73 nmol PS (0.05 mg PS|TiO₂), and mass, 1.5 µg PS, were deposited on the WE surface to assess which coating provides the highest sensitivity.

The thickness of the coating, which is function of the amount of TiO₂ particles deposited on the surface can influence the obtained photocurrent responses.[4] Therefore, the photocurrent responses of the ZnPcs were first compared when the amount of deposited PS|TiO₂ was 0.05 mg (Figure 7.A). Indeed, no significant increase in the photoresponse upon the addition of phenol was observed for $H_{16}PcZn|TiO_2$ and $F_{16}PcZn|TiO_2$ which was the result of the aggregation of the PS on the TiO₂ surface leading to a diminishing ¹O₂ production.[7]

This is in contrast with $F_{52}PcZn|TiO_2$ and $F_{64}PcZn|TiO_2$: the photocurrent increased 12 times for $F_{52}PcZn|TiO_2$ and 6.4 times for $F_{64}PcZn|TiO_2$. This higher increase in response for $F_{52}PcZn$ is explained by its higher ¹O₂ production and higher extinction coefficient at 655 nm (Table S1) compared to $F_{64}PcZn$. The blank responses (buffer solution) were also higher in the case of $F_{52}PcZn$ as these responses were caused by the direct reduction of ¹O₂ at the electrode

surface.[4] The higher deposited moles of PS in Figure 7.A, which was 0.85 nmol for $F_{52}PcZn|TiO_2$-coatings and 0.73 nmol for $F_{64}PcZn|TiO_2$, did not significantly influence these elevated obtained photocurrent responses for $F_{52}PcZn$. When 0.73 nmol $F_{52}PcZn$ was deposited on the surface, the photocurrent response of phenol remained mainly unaltered (Figure 7.B). Even when the amount of deposited PS was altered so that the absorbance at 655 nm was equal for $F_{52}PcZn|TiO_2$ and $F_{64}PcZn|TiO_2$, $F_{52}PcZn|TiO_2$ still provided the highest sensitivity for the detection of phenol (Figure S14). A slightly lower phenol photoresponse of -82 ± 6 nA was noted in this condition since the detection of phenol was solely dependent on the ¹O₂ production of the PS. Therefore, it is concluded that the use of $F_{52}PcZn|TiO_2$ results in the highest sensitivity for the sensing of phenol. Nonetheless, both $F_{52}PcZn|TiO_2$ and $F_{64}PcZn|TiO_2$ coatings showed high stability in the measurement of 1 µmol L⁻¹ phenol when their respectively modified SPEs were subjected to multiple illuminations (Figure S15).
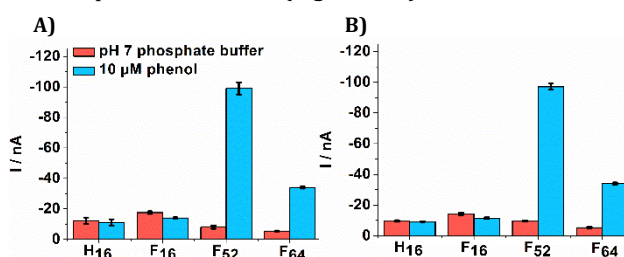

Figure 7. Photocurrent response of ItalSens SPE-coatings of 3 wt % $H_{16}PcZn|TiO_2$ (H_{16}), $F_{16}PcZn|TiO_2$ (F_{16}), $F_{52}PcZn|TiO_2$ (F_{52}) and $F_{64}PcZn|TiO_2$ (F_{64}) in pH 7 phosphate buffer (N = 3) in the presence (blue) and absence (red) of 10 µmol L⁻¹ phenol. (A) The same amount of PS|TiO₂ was deposited (0.05 mg) and (B) the same number of moles of PS (0.73 nmol) was deposited on the surface. The applied potential was -0.1 V vs Ag pseudo-reference electrode.

A calibration plot for the detection of phenol was made using $F_{52}PcZn|TiO_2$ (Figure S16). An LOD of 0.01 µmol L⁻¹ and sensitivity of 1.5 A L mol⁻¹ cm⁻² was determined. The linear dynamic range was between 0.01 and 1 µmol L⁻¹. This LOD demonstrates the high sensitivity of the sensor compared to other electrochemical techniques (Table S3).

CONCLUSIONS

Insights in the role of n in a series of fluorinated PSs, F_nPcZn, in the ¹O₂ generation and photoelectrochemical response for phenol were obtained. A 20:80 vol % EtOH:toluene, which led to well isolated PS molecules (except for $F_{16}PcZn$) was used. ¹O₂ production by F_nPcZn is best ranked using traps, less so by EPR using TEMP since TEMP could photoreduce the highly electron deficient F_nPcZn, a process that is more pronounced as n increases from 16 to 64, reducing the ¹O₂ production. The sensitivity of the photoelectrochemical sensor is largely determined by the ¹O₂ production by the PS itself, which in turn, depends on PS structural factors. The highest sensitivity for phenol sensing was obtained with the bulky $F_{52}PcZn|TiO_2$-coatings, the planar $H_{16}PcZn$ and $F_{16}PcZn$, which can aggregate on the TiO₂ carrier exhibited the lowest. The bulkiest $F_{64}PcZn|TiO_2$-coating was slightly less active relative to the $F_{52}PcZn|TiO_2$-coating, probably due to its relative diminished ability to bond to the

support. The obtained insights will help Pc research in general by showing which probing tools can be used to investigate $^1O_2$ formation. This is beneficial for designing efficient sensors as well as for other, $^1O_2$-based applications.

ASSOCIATED CONTENT

Supporting Information

The Supporting Information is available free of charge on the ACS Publications website.
Supporting information on reaction equations, synthesis, UV-Vis extinction coefficients, DMA and TEMPO experiments, UV-Vis measurements in 250 μL cuvette, leaching experiments and photoelectrochemical currents and responses. (file type, i.e., PDF)

AUTHOR INFORMATION

Corresponding Author

* E-mail: karolien.dewael@uantwerpen.be

Author Contributions

The manuscript was written through contributions of all authors.

ACKNOWLEDGMENT

REFERENCES

(1) Moons, H.; Lapok, L.; Loas, A.; Van Doorslaer, S.; Gorun, S. M. Synthesis, X-ray Structure, Magnetic Resonance, and DFT Analysis of a Soluble Copper(II) Phthalocyanine Lacking C-H Bonds. *Inorg Chem* **2010**, *49* (19), 8779-8789.

(2) Minnes, R.; Weitman, H.; Lee, H. J.; Gorun, S. M.; Ehrenberg, B. Enhanced acidity, photophysical properties and liposome binding of perfluoroalkylated phthalocyanines lacking C-H bonds. *Photochem Photobiol* **2006**, *82* (2), 593-599.

(3) Marais, E.; Klein, R.; Antunes, E.; Nyokong, T. Photocatalysis of 4-nitrophenol using zinc phthalocyanine complexes. *J Mol Catal A Chem* **2007**, *261* (1), 36-42.

(4) Trashin, S.; Rahemi, V.; Ramji, K.; Neven, L.; Gorun, S. M.; De Wael, K. Singlet oxygen-based electrosensing by molecular photosensitizers. *Nat Commun* **2017**, *8*.

(5) Neven, L.; Shanmugam, S. T.; Rahemi, V.; Trashin, S.; Sleegers, N.; Carrion, E. N.; Gorun, S. M.; De Wael, K. Optimized Photoelectrochemical Detection of Essential Drugs Bearing Phenolic Groups. *Anal Chem* **2019**, *91* (15), 9962-9969.

(6) Moons, H.; Loas, A.; Gorun, S. M.; Van Doorslaer, S. Photoreduction and light-induced triplet-state formation in a single-site fluoroalkylated zinc phthalocyanine. *Dalton Trans* **2014**, *43* (40), 14942-14948.

(7) Gerdes, R.; Lapok, L.; Tsaryova, O.; Wohrle, D.; Gorun, S. M. Rational design of a reactive yet stable organic-based photocatalyst. *Dalton Trans* **2009**, (7), 1098-1100.

(8) Bench, B. A.; Beveridge, A.; Sharman, W. M.; Diebold, G. J.; van Lier, J. E.; Gorun, S. M. Introduction of bulky perfluoroalkyl groups at the periphery of zinc perfluorophthalocyanine: Chemical, structural, electronic, and preliminary photophysical and biological effects. *Angew Chem Int Edit* **2002**, *41* (5), 748-750.

(9) Keizer, S. P.; Mack, J.; Bench, B. A.; Gorun, S. M.; Stillman, M. J. Spectroscopy and electronic structure of electron deficient zinc phthalocyanines. *J Am Chem Soc* **2003**, *125* (23), 7067-7085.

(10) Spiller, W.; Kliesch, H.; Wohrle, D.; Hackbarth, S.; Roder, B.; Schnurpfeil, G. Singlet oxygen quantum yields of different

photosensitizers in polar solvents and micellar solutions. *J Porphyr Phthalocyanines* **1998**, *2* (2), 145-158.

(11) Nardi, G.; Manet, I.; Monti, S.; Miranda, M. A.; Lhiaubet-Vallet, V. Scope and limitations of the TEMPO/EPR method for singlet oxygen detection: the misleading role of electron transfer. *Free Radic Biol Med* **2014**, *77*, 64-70.

(12) Nosaka, Y.; Nosaka, A. Y. Generation and Detection of Reactive Oxygen Species in Photocatalysis. *Chem Rev* **2017**, *117* (17), 11302-11336.

(13) Han, S. K.; Hwang, T. M.; Yoon, Y.; Kang, J. W. Evidence of singlet oxygen and hydroxyl radical formation in aqueous goethite suspension using spin-trapping electron paramagnetic resonance (EPR). *Chemosphere* **2011**, *84* (8), 1095-1101.

(14) Wu, W. T.; Zhang, Q. G.; Wang, X. K.; Han, C. C.; Shao, X. D.; Wang, Y. X.; Liu, J. L.; Li, Z. T.; Lu, X. Q.; Wu, M. B. Enhancing Selective Photooxidation through Co-Nx-doped Carbon Materials as Singlet Oxygen Photosensitizers. *ACS Catal* **2017**, *7* (10), 7267-7273.

(15) Cerny, J.; Karaskova, M.; Rakusan, J.; Nespurek, S. Reactive oxygen species produced by irradiation of some phthalocyanine derivatives. *J Photochem Photobiol A: Chem* **2010**, *210* (1), 82-88.

(16) Epelde-Elezcano, N.; Martinez-Martinez, V.; Pena-Cabrera, E.; Gomez-Duran, C. F. A.; Arbeloa, I. L.; Lacombe, S. Modulation of singlet oxygen generation in halogenated BODIPY dyes by substitution at their meso position: towards a solvent-independent standard in the vis region. *RSC Adv* **2016**, *6* (48), 41991-41998.

(17) Kluson, P.; Drobek, M.; Kalaji, A.; Zarubova, S.; Krysa, J.; Rakusan, J. Singlet oxygen photogeneration efficiencies of a series of phthalocyanines in well-defined spectral regions. *J Photochem Photobiol A: Chem* **2008**, *199* (2-3), 267-273.

(18) Albiter, E.; Alfaro, S.; Valenzuela, M. A. Photosensitized oxidation of 9,10-dimethylanthracene with singlet oxygen by using a safranin O/silica composite under visible light. *Photochem Photobiol Sci* **2015**, *14* (3), 597-602.

(19) Garcia, A. M.; Alarcon, E.; Munoz, M.; Scaiano, J. C.; Edwards, A. M.; Lissi, E. Photophysical behaviour and photodynamic activity of zinc phthalocyanines associated to liposomes. *Photochem Photobiol Sci* **2011**, *10* (4), 507-514.

(20) Carrión, E. N.; Loas, A.; Patel, H. H.; Pelmuş, M.; Ramji, K.; Gorun, S. M. Fluoroalkyl phthalocyanines: Bioinspired catalytic materials. *J Porphyr Phthalocyanines* **2018**, *22* (05), 371-397.

(21) Jiang, H.; Hu, P.; Ye, J.; Ganguly, R.; Li, Y. X.; Long, Y.; Fichou, D.; Hu, W. P.; Kloc, C. Hole Mobility Modulation in Single-Crystal Metal Phthalocyanines by Changing the Metal-pi/pi-pi Interactions. *Angew Chem Int Ed* **2018**, *57* (32), 10112-10117.

(22) Ogunsipe, A.; Chen, J. Y.; Nyokong, T. Photophysical and photochemical studies of zinc(II) phthalocyanine derivatives - effects of substituents and solvents. *New J Chem* **2004**, *28* (7), 822-827.

(23) Ogunsipe, A.; Maree, D.; Nyokong, T. Solvent effects on the photochemical and fluorescence properties of zinc phthalocyanine derivatives. *J Mol Struct* **2003**, *650* (1-3), 131-140.

(24) Sun, Y. L.; Li, X. G.; Wang, S. R.; Zhang, L. J.; Ma, F. Synthesis, Spectral Properties of Zinc Hexadecafluorophthalocyanine (ZnPcF16) and Its Application in Organic Thin Film Transistors. *Mater Trans* **2017**, *58* (1), 103-106.

(25) Diaz-Torres, R.; Alvarez, S. Coordinating ability of anions and solvents towards transition metals and lanthanides. *Dalton Trans* **2011**, *40* (40), 10742-10750.

(26) Batat, P.; Bayar, M.; Pur, B.; Coker, E.; Ahsen, V.; Yuksel, F.; Demirel, A. L. The optical characterization of metal-mediated aggregation behaviour of amphiphilic Zn(II) phthalocyanines. *Phys Chem Chem Phys* **2016**, *18* (23), 15574-15583.

(27) Takajo, T.; Kurihara, Y.; Iwase, K.; Miyake, D.; Tsuchida, K.; Anzai, K. Basic Investigations of Singlet Oxygen Detection Systems with ESR for the Measurement of Singlet Oxygen Quenching Activities. *Chem Pharm Bull* **2020**, *68* (2), 150-154.

(28) Yamakoshi, Y.; Umezawa, N.; Ryu, A.; Arakane, K.; Miyata, N.; Goda, Y.; Masumizu, T.; Nagano, T. Active oxygen species generated from photoexcited fullerene (C-60) as potential medicines: $O_2^{\bullet-}$ versus $^1O_2$. *J Am Chem Soc* **2003**, *125* (42), 12803-12809.

(29) Geerdink, R. B.; van den Hurk, R. S.; Epema, O. J. Chemical oxygen demand: Historical perspectives and future challenges. *Anal Chim Acta* **2017**, *961*, 1-11.

(30) Emerson, E. The Condensation of Aminoantipyrine. II. A New Color Test for Phenolc Compounds. *J Org Chem* **1943**, *08* (5), 417-428.